

# DISTANT DIPOLE-DIPOLE INTERACTIONS AND THE STRUCTURE OF DEFECTS AND IMPURITIES IN SILICON

E. G. SIEVERTS and C. A. J. AMMERLAAN

*Natuurkundig Laboratorium der Universiteit van Amsterdam Valckenierstraat 65,  
NL-1018 XE Amsterdam, The Netherlands*

*(Received February 13, 1989)*

With EPR and ENDOR hyperfine interactions with silicon and impurity nuclei have been determined for many different defects and impurity centers in silicon. A standard interpretation is mostly given with an LCAO description, as introduced into this field by Watkins and Corbett. Usually, this method only includes contributions from atomic orbitals centered on the pertinent nuclei. The anisotropic part of the hyperfine interaction arises from dipole-dipole interaction due to p-(or d-)orbitals. Only under special circumstances perceptible contributions are made by dipole-dipole interaction between nuclei and unpaired spin density which is localized at other nuclei. If this is the case, additional information on the detailed structure of the defects can be obtained. Several examples are discussed in this paper, both for vacancy-related defects and for transition metal impurities in silicon. For the vacancy we derive a lattice relaxation which is opposite to theoretical predictions.

## I INTRODUCTION

During the past 30 years magnetic resonance techniques have played an important role in the identification of defects and impurities in silicon, as well as in the elucidation of their detailed atomic and electronic structure.<sup>1-7</sup> Observations of hyperfine interactions between unpaired electron spin and nuclei with a magnetic moment have played a prominent part in this work. Such observations could be made, both with electron paramagnetic resonance (EPR) in which transitions between electron spin states are induced, and with electron nuclear double resonance (ENDOR) in which nuclear spin states are changed. With EPR hyperfine interactions can only be observed if the interaction is large compared to the inhomogeneously broadened line width of the resonance lines and/or if the isotopic abundance of the magnetic nucleus is not too small. In limiting cases there is of course a correlation between these two factors. The much higher resolving power of ENDOR can reveal hyperfine interactions which are at least two orders of magnitude smaller.

In 1959 for the first time well resolved hyperfine interactions from EPR spectra in electron irradiated silicon were reported by Watkins, Corbett, and Walker.<sup>8</sup> These originated from the 100% abundant <sup>31</sup>P nuclei in what was (already correctly) supposed to be the phosphorus-vacancy complex, and from the 4.7% abundant <sup>29</sup>Si nuclei in both this defect and the oxygen-vacancy complex. In the same year small hyperfine interactions with a large number of <sup>29</sup>Si nuclei, surrounding the group V shallow donor impurities in silicon, which could only be observed with ENDOR, were reported as well.<sup>9</sup> Only much later ENDOR was for the first time applied to radiation defects in silicon.<sup>10</sup>

An important tool for the interpretation of hyperfine interactions in vacancy related defects in silicon was developed when Watkins and Corbett introduced

molecular orbitals which were built from linear combinations of atomic orbitals (LCAO) to describe the broken bond states in which the unpaired defect electron was found.<sup>11,12</sup> In this one-electron approach the wave function of the defect electron is described as a molecular orbital which is a sum of linear combinations of atomic s- and p-orbitals over several atomic sites  $i$

$$\Psi = \sum_i \eta_i (\alpha_i \psi_{s,i} + \beta_i \psi_{p,i}). \quad (1)$$

When deriving formulas for the hyperfine interactions between an electron in such a wave function and a nuclear spin, in general only the atomic orbitals centered at the same nucleus are considered. In most situations this gives a sufficiently accurate description, as dipole-dipole interaction from distant spin can mostly be neglected with respect to contributions from the own atomic orbitals. There are special circumstances, however, in which these distant contributions can play a prominent role. These circumstances and examples in which they prevail, will be discussed in this paper. In these cases the observed directions of the principal values or the axial directions of the hyperfine interactions can give important clues to the relative positions of constituent atoms of the defect.

## II DIPOLE-DIPOLE INTERACTION

Experimentally observed hyperfine interaction tensors  $\vec{A}_i$  can be written as  $\vec{A}_i = a_i \vec{1} + \vec{B}_i$ , where  $\vec{B}_i$  is a purely anisotropic (traceless) tensor. The isotropic part  $a_i$  is proportional to the probability density of the electron wave function at the site of the magnetic nucleus. In an LCAO description this means that it is related to the atomic s orbitals at the nucleus.

The dipole-dipole interaction between the magnetic moments of a nuclear spin and an electronic spin distribution can be described by the spin Hamiltonian term

$$\mathcal{H} = \vec{S} \cdot \vec{B} \cdot \vec{I} \quad (2)$$

with a traceless tensor  $\vec{B}$  with components

$$B_{ij} = \frac{\mu_0}{4\pi} g\mu_B g_N \mu_N \left\langle \Psi \left| \frac{3x_i x_j}{r^5} - \frac{\delta_{ij}}{r^3} \right| \Psi \right\rangle. \quad (3)$$

This is the quantummechanical equivalent of the classical dipole-dipole interaction and involves integration over the wave function  $\Psi$  which describes the electron spin distribution.

For an electron spin in a point charge Eq. (3) simply reduces to an axially symmetric tensor with principal values  $(2b, -b, -b)$  and

$$b = \frac{\mu_0}{4\pi} g\mu_B g_N \mu_N \frac{1}{R^3}, \quad (4)$$

in which  $R$  is the distance between the point charge and the nucleus, and where the axial direction is along the connection line between these two. If only a fraction of an electron is present, an appropriate multiplication factor must be included in Eq. (4).

If an electron spin is described by an LCAO wave function as given in Eq. (1), and if only orbitals centered on the pertinent nucleus are considered, only p-orbitals contribute to the dipole-dipole interaction. They give rise to an axially symmetric tensor as well, directed along the lobe of the p-orbital and with

$$b_i = \frac{\mu_0}{4\pi} g\mu_B g_N \mu_N \frac{2}{5} \eta_i^2 \beta_i^2 \langle r^{-3} \rangle_p. \quad (5)$$

In cases where d-orbitals are included in the wave function, a similar formula follows, with a factor 2/7 instead of 2/5.

Substitution of numerical values in Eqs. (4) and (5) supports the importance of the orbital contribution over the distant dipole-dipole interaction. A silicon atomic 3p-orbital gives rise to a factor  $2/5 \langle r^{-3} \rangle_p = 7.264 \times 10^{30} \text{ m}^{-3}$ <sup>13</sup> and hence  $b_i = 114 \text{ MHz}$  for a <sup>29</sup>Si nucleus, whereas an electron in a point charge at nearest neighbor distance gives only a factor  $R^{-3} = 0.077 \times 10^{30} \text{ m}^{-3}$  and hence  $b = 1.2 \text{ MHz}$ . This means that only for p-orbital localizations  $\eta^2 \beta^2 < 1\%$  at a nearest neighbor site of a full electron spin, the distant interaction becomes important. As the distant interaction falls off with  $R^{-3}$ , limiting localizations at more remote neighbor sites are even appreciably smaller. This means that only under special circumstances the distant interaction can have any perceptible effect at all. A necessary condition for its observation is in any case that an appreciable fraction of an electron spin is very localized at a particular site, not too far from the nucleus with which a hyperfine interaction is experimentally observed. As a result, for delocalized shallow defects and impurities, it need not to be considered at all. For lattice defects with spin localized in dangling bonds or for transition metal impurities with a high degree of localization at the transition metal atom, on the other hand, effects may be observed.

As an example the divacancy in silicon can be considered. ENDOR measurements have been performed on its positive ( $V_2^+$ ) and negative ( $V_2^-$ ) charge state.<sup>10,14</sup> In both cases a considerable number of hyperfine interaction tensors have been observed. For both charge states the unpaired defect electron has a localization of approximately 30% in each of the two dangling bonds at both sides of the two vacancies. Taking these for simplicity as point charges, they will give rise to an interaction with  $b \approx 300 \text{ kHz}$  at their nearest neighbor lattice sites. Because of the low symmetry of the divacancy, the observed hyperfine interactions fall apart in only two groups, those from sites in the mirror plane of the defect, called M-class interactions, and those from outside the plane, called G-class interactions. In both groups however several interactions have been observed with larger anisotropic parts  $b$ . For  $V_2^+$  6 G-class tensors and for  $V_2^-$  8 G-class tensors have  $b > 300 \text{ kHz}$ . For the M-class tensors (with exception of the largest which represents the dangling bonds themselves) these numbers are 8 and 4, respectively. This means that it is unlikely that the interaction with a nearest neighbor is small enough to allow observation of distant dipole-dipole effects, and if one happens to be small, there is no means to recognize that it is a close neighbor. This conclusion had already been drawn earlier.<sup>15</sup>

The reason for the relatively large hyperfine interactions in the neighborhood of dangling bond atoms is probably some kind of spin transfer through the covalent bonds of the silicon lattice.<sup>16</sup> This means that an additional condition must be satisfied without which the distant dipole-dipole effects can not be recognized. In the rest of this paper we will discuss three different cases.

- 1) For symmetry reasons the localization of the unpaired spin has to be zero in a special plane or on a special axis.
- 2) A large spin localization at a lattice site close by is not transferred to certain lattice sites, because the geometry of the defect structure prevents it.
- 3) The electron spin is strongly localized, but not in a dangling bond.

Effects of distant dipole-dipole interaction are by far the most prominent in the first case. The two most striking examples are the negative charge states of both the single vacancy and the oxygen-vacancy complex.<sup>16, 17</sup> Both these examples will be discussed in more detail in the next section. Another example which we will discuss is a vacancy with two nearest neighbor phosphorus atoms.<sup>18</sup> Examples in which the geometry of the defect plays an important role all concern interactions with impurity atoms, i.e. in the boron-vacancy, the phosphorus-vacancy and the antimony-vacancy complexes.<sup>19-21</sup> Good examples of localized defects without dangling bonds, finally, are the various interstitial transition metal impurities in silicon.<sup>22</sup>

### III SYMMETRY FORBIDDEN SITES

#### A. Vacancy and Oxygen-Vacancy Complexes

When the vacancy in silicon is considered as just a missing atom, it is expected that this defect has tetrahedral symmetry. If an energy level diagram is drawn for this structure with electrons in dangling bond orbitals on the four nearest neighbors, it follows that the paramagnetic  $V^-$  state has an orbitally degenerate ground state. Consequently Jahn-Teller distortion is bound to occur, resulting in a state of rhombic  $2mm$  point-group symmetry, as shown in Figure 1. In this symmetry there are two perpendicular, inequivalent  $\{011\}$  mirror planes. In the negative charge state, the unpaired defect electron is found in the antisymmetric combination a-d of the two dangling bond orbitals on the atoms labelled a and d. They determine one of the mirror planes,  $(0\bar{1}1)$  in Figure 1. As a result of the antisymmetry, the other mirror plane,  $(011)$ , will be a nodal plane of the defect wave function.

Due to the relatively high  $2mm$ /point-group/symmetry, hyperfine interactions from four different types of lattice sites can experimentally be distinguished. For two types the sites are in the nodal plane. The identification as a nodal plane means that at least the Fermi contact interaction, which arises from s-orbitals in the LCAO description, should be vanishingly small for sites in this plane. The only allowed contributions to an LCAO wave function are p-orbitals perpendicular to the nodal plane. However, all of the experimentally determined hyperfine interactions in this plane of the vacancy contain contributions which result from more than just such perpendicular p-orbitals. The additional contributions, although not zero, are found to be at least an order of magnitude smaller indeed, than those outside the plane.<sup>16</sup> This indicates that the interaction does not result from the LCAO wave function of the unpaired electron in the usual way, but from second-order effects only. One of these second-order effects, and the most important for the anisotropic part of the observed hyperfine interactions, is the distant dipole-dipole effect.

For the negative oxygen-vacancy complex ( $OV^-$ ) exactly the same symmetry considerations are valid as for  $V^-$ .<sup>12</sup> Moreover, the hyperfine interactions as observed with ENDOR are very similar to those of  $V^-$ . For 2/3 of the 50 observed hyperfine tensors a direct correspondence with a  $V^-$  interaction could be

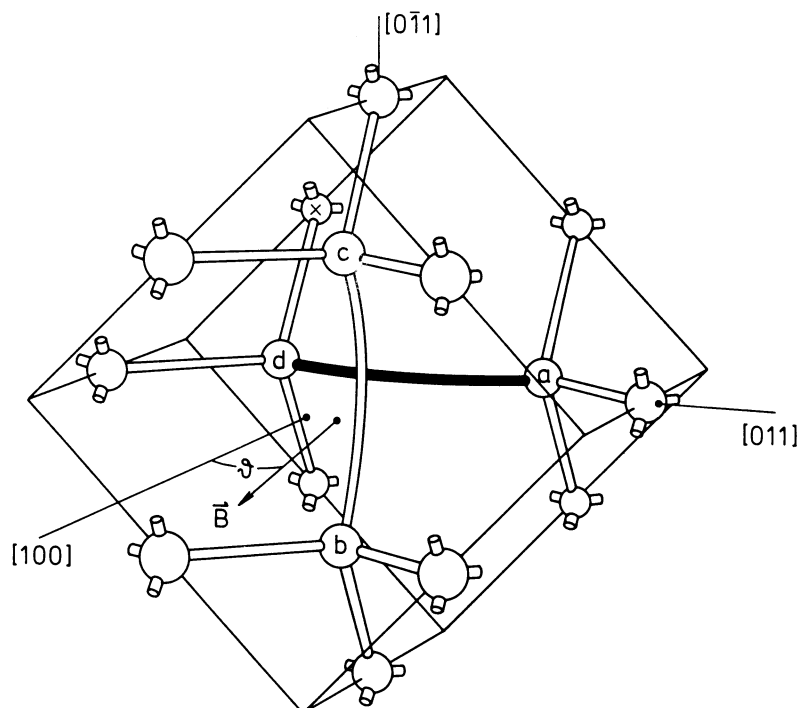


FIGURE 1 Model of the vacancy in silicon.

established.<sup>17</sup> A number of these are in the forbidden (011) mirror plane. Figure 1 can easily be used as a model for  $OV^-$  as well, if we imagine an oxygen atom situated in the bent bond between the silicon atoms b and c.

For both the vacancy and the oxygen-vacancy complex by far the largest hyperfine interactions, and hence the largest electron spin localizations, are found in dangling bonds on the two neighbor atoms a and d of the vacancy. First we assume that this spin is localized in point charges on these atoms. The dipole-dipole interactions at other lattice sites can easily be calculated by the use of Eq. (4), application of appropriate transformations, and addition of the cartesian tensors which result from each of the two dangling bonds. From ENDOR experiments it followed that also a reasonable amount of spin is found on two next-nearest neighbors of the vacancy,  $[022]$  and  $[0\bar{2}\bar{2}]$ , 5.9% on each for  $V^-$  and 4.4% for  $OV^-$ .<sup>16,17</sup> In actual calculations which have been performed, spin on these two atoms has also been included. These calculations have primarily been performed for nuclei at lattice sites in the forbidden (011) plane. Spin localizations as used in these calculations are given in Table I. Results of the calculations in Table II are only given for  $OV^-$ . Calculated interactions for  $V^-$  were only slightly different, at the average  $\sim 10\%$  smaller, with almost identical principal directions. Given are principal values and the angle between the first principal direction and  $[100]$ . Calculations have not only been performed for spin in point charges, indicated by "point", but also for more realistic spin distributions. In that case Slater-type orbitals

$$\phi_{3s} = n_s r^2 \exp\left(-\alpha_s \frac{r}{a_0}\right),$$

$$\phi_{3px} = n_p x r \exp\left(-\alpha_p \frac{r}{a_0}\right) \quad (6)$$

and similar expressions for  $\phi_{3py}$  and  $\phi_{3pz}$  have been substituted in Eq. (3). Integration over these orbitals can easily be performed when using the series expansion derived by Ammerlaan and Wolfrat.<sup>23</sup> Although even these orbitals tend to be somewhat too localized, the results, especially for sites close to the dangling bonds, are much more realistic than those from point charges. In Table II these results are indicated by "slater".

TABLE I  
Spin distribution on the four atoms with highest localization for  $V^-$  and  $OV^-$ <sup>16,17</sup>

	[ $\bar{1}11$ ] and [ $\bar{1}\bar{1}\bar{1}$ ]			[022] and [0 $\bar{2}\bar{2}$ ]		
	$\eta^2$	$\alpha^2$	$\beta^2$	$\eta^2$	$\alpha^2$	$\beta^2$
$V^-$	0.273	0.284	0.716	0.059	0.185	0.815
$OV^-$	0.300	0.302	0.698	0.044	0.195	0.805

TABLE II

Calculated dipole-dipole interactions at sites in the "forbidden" (011) plane of  $V^-$  or  $OV^-$ . Calculations have been made for a point charge model ("point") and using Slater type orbitals ("slater") with parameter values  $\alpha_s = 1.87$  and  $\alpha_p = 1.60$ .<sup>23</sup> For position [0.75, 0, 0] the  $^{17}O$  nuclear magnetic moment has been used, for other positions the moment of  $^{29}Si$ . The spin distribution for  $OV^-$  has been taken; results for the  $V^-$  distribution were slightly smaller. Given are principal values  $B_i$  in kHz and the angle  $\theta$  between  $B_1$  and [100] in the (011) plane

Position	Type	$B_1$	$B_2$   [011]	$B_3$	$\theta$ (deg)
[0.75, 0, 0]	point	-183.8	-41.7	+225.5	0
	slater	-387.6	-9.8	+397.4	0
[1, -1, 1]	point	-202.3	+17.6	+184.7	36.0
	slater	-346.1	+88.2	+257.9	39.0
distorted	slater	-1180	+480	+700	30.9
[0, -2, 2]	point	-153.9	+41.1	+112.8	71.7
	slater	-208.8	+75.3	+133.5	75.6
[-4, 0, 0]	point	-156.3	+46.9	+109.4	0
	slater	-162.6	+62.7	+99.9	0
[-3, -1, 1]	point	-213.9	+39.2	+174.7	-34.9
	slater	-255.4	+88.3	+167.1	-31.9
[-4, -2, 2]	point	-81.4	+32.1	+49.3	-42.8
	slater	-82.2	+35.3	+46.9	-40.8
[4, 0, 0]	point	-54.0	+20.9	+33.1	0
	slater	-65.4	+27.6	+37.8	0
[5, -1, 1]	point	-32.2	+13.8	+18.4	13.7
	slater	-36.7	+16.4	+20.3	14.0
[4, -2, 2]	point	-38.3	+16.1	+22.2	30.4
	slater	-43.9	+19.4	+24.5	31.2

Observed hyperfine interactions in this forbidden mirror plane are those labelled Mbc and T in Refs. 16 and 17. For  $V^-$ , five Mbc and two T tensors have been observed, for  $OV^-$ , six Mbc and only one T tensor. Based on the calculated dipole-dipole interactions all tensors, except one of  $V^-$  and one of  $OV^-$ , could be identified with certain lattice sites. For these tensors, the identification, the principal values, and the angle between the first principal direction and  $[100]$  are given in Table III. For  $OV^-$ , moreover, results for the oxygen atom, as obtained from an ENDOR experiment on a  $^{17}O$  isotopically enriched sample, are included.<sup>24</sup> In Figure 2 the forbidden (011) planes for  $V^-$  and  $OV^-$  are shown, with the identified lattice sites shown shaded.

TABLE III  
Experimental anisotropic hyperfine interactions for sites in the forbidden (011) plane of  $V^-$  and  $OV^-$ .  
Given are principal values  $B_i$  (in kHz) and the angle  $\theta$  between  $B_1$  and  $[100]$  in the (011) plane

Position	Tensor	$B_1$	$B_2$   [011]	$B_3$	$\theta$ (deg)
[0.75, 0, 0]	$OV^-:^{17}O$	+ 1376.6	- 3983.0	+ 2606.4	0 <sup>a</sup>
[1, -1, 1]	$V^-:Mbc5$	- 1360.9	+ 606.1	+ 754.8	31.3 <sup>b</sup>
	$OV^-:Mbc1$	- 380.1	+ 227.0	+ 153.1	40.5 <sup>a</sup>
[0, -2, 2]	$V^-:Mbc3$	- 134.8	+ 103.2	+ 31.6	66.9
	$OV^-:Mbc4$	- 142.5	+ 122.9	+ 19.6	68.6
[-4, 0, 0]	$V^-:T1$	- 148.2	+ 41.8	+ 106.4	0
	$OV^-:T1$	- 164.1	+ 32.0	+ 132.1	0
[-3, -1, 1]	$V^-:Mbc1$	- 352.5	+ 79.4	+ 273.1	- 31.1
	$OV^-:Mbc3$	- 344.5	+ 49.9	+ 294.6	- 23.4
[-4, -2, 2]	$V^-:Mbc4$	- 63.7	+ 39.7	+ 24.0	- 40.9
	$OV^-:Mbc2$	- 115.1	+ 48.4	+ 66.7	- 40.8
[4, 0, 0]	$V^-:T2$	- 32.1	- 33.3	+ 65.4	0 <sup>a</sup>
[4, -2, 2]	$OV^-:Mbc5$	- 61.1	+ 17.7	+ 43.4	35.2

<sup>a</sup>After subtraction of calculated values (Slater), an almost perfect [011] axial tensor remains.

<sup>b</sup>Corresponds very well with calculated values for strong distortion of nearest neighbors.

Not all tensors give satisfactorily matching results, especially not those which are identified with sites close to the vacancy. However, we can consider the calculated dipole-dipole interaction as a known contribution. The results which remain after subtraction of this contribution are in most of the cases very well [011] axial, and thus symmetry allowed in the LCAO description.

For the atoms b and c in  $V^-$  this does not work. The observed tensor components of the interaction which we expect to belong to these atoms are just much too large. An explanation may be that even Slater orbitals are too localized on the dangling bond atoms, whereas the actual wave function on the atoms a and d extends much farther inward towards the vacancy. However, such enhanced delocalization towards the vacancy is not required for the oxygen-vacancy complex. On the other hand, a very satisfactory result can also be obtained if we assume that appreciable lattice relaxations occur at the nearest neighbors of the vacancy. In Table II results from a calculation after distortion are shown which correspond fairly well with the experimental data. As a matter of fact, the positions of the two dangling bond atoms a and d and the two forbidden plane atoms b and c have been varied in order to obtain a best fit with experiment. The required relaxation is rather large, about 1/3 of a bond length inward for all four atoms. The relaxation of the atoms a

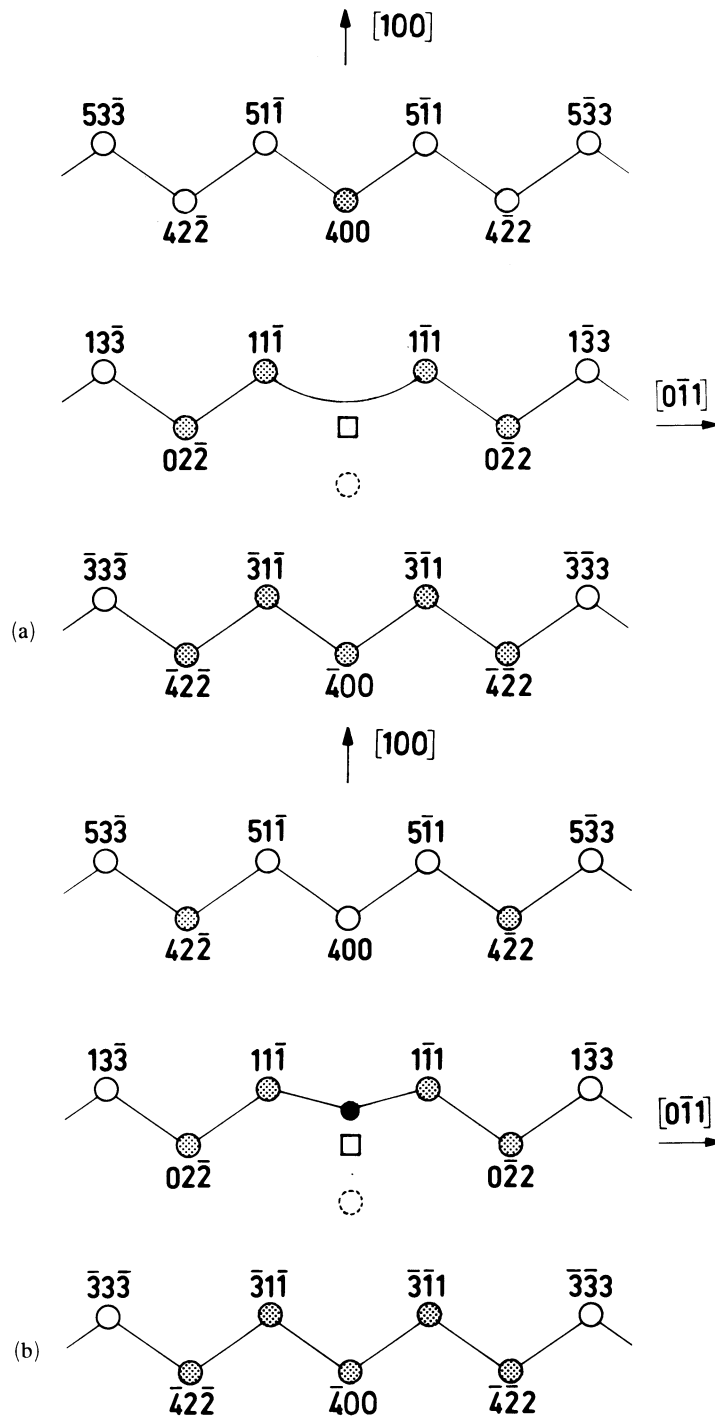


FIGURE 2 The forbidden (011) plane of (a) the vacancy and (b) the oxygen-vacancy complex in silicon. Atom sites with identified hyperfine interactions are shown shaded. The black ball is an oxygen atom. The dashed circle shows where dangling bond atoms a and d are located above and below the (011) plane.

and d may be somewhat overestimated, if the spin in the dangling bonds at these atoms is actually more delocalized towards the vacancy than in a Slater orbital. However, the distortion of the atoms b and c with the magnetic nuclei should indeed be of this order of magnitude. Although an inward relaxation seems reasonable at first sight, theoretical calculations of the stable configuration of the lattice vacancy arrive unvaryingly at an outward relaxation.<sup>25-27</sup> However, the correspondence between the experimentally obtained data and the calculated dipole-dipole interaction is rather convincing, so that one may wonder how reliable the theoretical predictions are.

On the basis of these results we may thus conclude that most Mbc and T type interactions of  $V^-$  and  $OV^-$  can indeed be explained and hence be identified by distant dipole-dipole interaction. Figure 2 shows that no relevant sites in the forbidden plane are missing either. For the vacancy, moreover, a nearest neighbor lattice relaxation opposite to accepted theoretical belief is suggested.

### B. Phosphorus-Vacancy-Phosphorus Complex

In highly phosphorus-doped silicon, after electron irradiation, several paramagnetic defects have been observed which showed hyperfine interactions from pairs of phosphorus atoms.<sup>18</sup> Especially for one of the EPR spectra, labelled NL1, the proposed model of a vacancy between two phosphorus atoms was considered to be well established. Its paramagnetic state is supposed to be the positive charge state  $PVP^+$ . Figure 1 can be taken as a model for this defect, if the atoms b and c are phosphorus atoms instead of silicon. From the g-tensor it followed that the defect has the same 2mm symmetry as  $V^-$  and  $OV^-$ . Moreover, the g-values of these three defects are very similar. Lee and Corbett have introduced a very useful two-dimensional presentation of g-values in an axial approximation where  $g_{\parallel}$  is plotted against  $g_{\perp}$ .<sup>28,3</sup> In such a plot spectrum NL1 falls exactly in between the spectra of  $V^-$  and  $OV^-$ . In EPR a very well-resolved hyperfine interaction with two silicon atoms is observed, which is also almost identical to the largest interactions in  $V^-$  and  $OV^-$ . Therefore, it is also identified as to arise from two broken bonds at the atoms a and d in Figure 1. The localization at each of them is 28.5%.

In the singly positive charge state the number of electrons of the system is the same as for  $V^-$  and  $OV^-$ . Consequently, a group theoretical treatment arrives at the same type of wave function for the unpaired electron, antisymmetric with respect to the plane of the two phosphorus atoms.<sup>29</sup> This means that the phosphorus atoms are in a nodal plane, in which only perpendicular p-orbitals are allowed. Yet, a well-resolved hyperfine interaction is observed in EPR, with an isotropic part  $a = 13.4$  MHz and an anisotropic part  $b = 0.15 \pm 0.05$  MHz.

Presented in the same way as the data in Table III, principal values of the anisotropic part of the interaction are:  $B_{1\parallel(100)} = 170$  kHz,  $B_{2\parallel(011)} = -280$  kHz,  $B_{3\parallel(0\bar{1}1)} = 110$  kHz. As the localization on the dangling bond atoms is the same as for  $V^-$  and  $OV^-$ , this should be compared with the calculated dipole-dipole interactions on the nearest neighbors, as given for position  $[1, -1, 1]$  in Table II. Because of the larger (and opposite) nuclear moment of  $^{31}\text{P}$  compared to  $^{29}\text{Si}$  these values must be multiplied by  $-2.04$ , however. For Slater orbitals this results in  $B_1 = 706$  kHz,  $B_2 = -180$  kHz, and  $B_3 = -526$  kHz. These numbers are only comparable in order of magnitude. Despite the relatively large uncertainty of the experimental values, this is not really satisfactory. Moreover, the calculated principal directions of  $B_2$  and  $B_3$  are different, the experimental ones being fixed by symmetry.

Because of the 100% abundance of the  $^{31}\text{P}$  isotope, hyperfine interactions in EPR are always observed with two P-nuclei at the same time. This interaction gives rise to a threefold splitting. The two outer EPR lines exhibit the actual hyperfine splitting, arising from states with the two nuclear spins parallel. As a result, in EPR only an average interaction with the overall 2mm defect symmetry can be determined, whereas the actual interaction with each of the P-nuclei is of lower symmetry. Information on the lower symmetry tensor components is in fact contained in a slight angular dependence of the central EPR line which arises from defects with the two nuclear spins antiparallel. However, in EPR this information is hidden in the broadening of this central line (see Appendix B of Ref. 29). These additional tensor components only influence the principal values  $B_1$  and  $B_3$ . One can easily substitute values which result for instance in  $B_1 = 700$  kHz and  $B_3 = -420$  kHz and principal directions with  $\theta \approx 40^\circ$  for  $B_1$ , in agreement with the calculated dipole-dipole interaction.

We therefore conclude that in this case the anisotropic part of the hyperfine interaction also results mostly from distant dipole-dipole interaction due to unpaired spin on the two dangling bond atoms. Due to the 100% abundance of  $^{31}\text{P}$ , its two times larger nuclear moment, and the apparently strong core polarization which causes the isotropic part of the hyperfine interaction, the interaction in the forbidden plane can even be observed in EPR.

#### IV DEFECT GEOMETRIES

##### A. Boron-Vacancy Complex

Of all EPR-identified impurity-vacancy complexes, the boron-vacancy complex is one of the most remarkable, as it has the boron atom at the next-nearest neighbor position of the vacancy. Moreover, it has the lowest possible, triclinic symmetry. This configuration was first suggested by Watkins<sup>30</sup> and later confirmed by ENDOR measurements on both boron and silicon nuclei.<sup>19</sup> The unpaired electron was found to be primarily located in a single dangling bond, say at atom a in Figure 1, with  $\eta^2 = 55\%$ . On atoms b and c respectively 4.8% and 5.1% is found, whereas at atom d no unpaired spin, or in any case less than 3%, is found (contrary to what the figure shows). The boron atom, finally, is located at the position  $[-2, -2, 0]$ , marked x in Figure 1.

Spin-density at neighboring sites of a defect is thought to be transferred mainly through the covalent bonds of the silicon lattice. At the nearest neighbor of the boron atom, atom d, practically no spin is located, whereas atom a is three bonds away, at the opposite end of a puckered six-ring of lattice sites. As a result, it is to be expected that only little of the observed hyperfine interaction at the boron atom is directly due to the LCAO wave function. Indeed a small interaction and different signs for a and b are found,  $a = 154.3$  kHz and  $b = -345.5$  kHz for the  $^{11}\text{B}$  nuclei. This small interaction indicates that the boron atom has almost the electronic structure of a silicon atom, so that it is actually a  $\text{B}^-\text{V}^+$ -complex, with the positive charge mainly at atom d. The different signs of a and b are not consistent with the LCAO model. An explanation can be given if we assume that the isotropic part mostly results from core polarization, whereas the anisotropic part mostly results from core polarization, whereas the anisotropic part b comes primarily from dipole-dipole interaction induced by the unpaired spin in the dangling bond at a. Calculations of dipole-dipole interaction at position x, due to

point charges and due to Slater orbitals at the atoms a, b, and c, have been performed in the same way as in Section III-A. It followed that a fairly good description of the observed value of b, its axial direction, and the deviation from axially could be given, if it was assumed that the orbitals and/or the atoms were extended towards the vacancy.<sup>19</sup>

Resuming, we note that in this example the spin density at a site close to the vacancy is low, because of the geometry and the electronic structure of the defect. The small resulting hyperfine interaction could still be recognized because it came from an impurity nucleus. The anisotropic part was satisfactorily explained by just distant dipole-dipole interaction.

### B. Phosphorus-Vacancy and Antimony-Vacancy Complex

The phosphorus-vacancy complex was one of the first radiation defects which was identified with EPR.<sup>8, 11, 20, 21</sup> Just as in the previous example, the unpaired spin is primarily located in a single dangling bond, with  $\eta^2 = 59\%$ . In comparison to the pertaining <sup>29</sup>Si hyperfine interaction, the observed <sup>31</sup>P hyperfine interaction is fairly small. With  $a = 27.95$  MHz and  $b = 1.90$  MHz, an LCAO analysis gives rise to a localization  $\eta^2 = 1\%$ , of which 29% is s-character. In Figure 3 it is shown that the axial direction deviates quite far from the usual  $\langle 111 \rangle$  direction, pointing almost to the unpaired spin in the dangling bond. This fact suggests already that dipole-dipole interaction with this spin may be important.

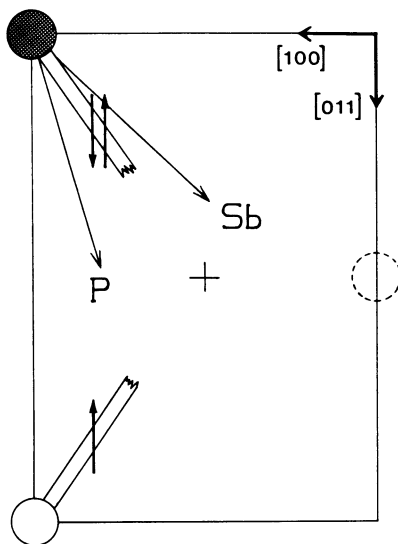


FIGURE 3 Detail of the phosphorus-vacancy or antimony-vacancy complex. Axes of impurity hyperfine interactions are indicated.

If we calculate the interaction at the phosphorus nucleus due to a point charge of 59% of an electron at the dangling bond atom at a distance of  $3.8 \text{ \AA}$ , we arrive at an axially symmetric interaction with  $b \approx 350$  kHz and its axis along the  $[011]$  direction. A Slater orbital gives a slightly larger interaction, with  $b \approx 480$  kHz and an axis  $5.5^\circ$  away from  $[011]$ . Comparison with the experimental data shows that the interaction is appreciably larger, but that the deviation of the axial direction can be accounted for by dipole-dipole effects. This is certainly the case if we assume a

wave function which is more extended towards the vacancy or a lattice distortion which brings the phosphorus atom and the dangling bond slightly closer together. If for instance a point charge is put in the dangling bond at the point to which the hyperfine axis points, distant dipole-dipole effects already account for almost 45% of the observed interaction.

For antimony-doped silicon a similar defect has been observed with EPR.<sup>21</sup> In this case the observed interaction with the dangling bond at the silicon atom is almost the same, the interaction with the antimony impurity atom is appreciably larger,  $a = 401$  MHz and  $b = 16.3$  MHz. These larger values can only partly be explained by the larger wave function parameters for antimony atomic orbitals, compared to phosphorus,<sup>13</sup> as this is partly counterbalanced by a smaller magnetic moment of the  $^{121}\text{Sb}$  nucleus in Eq. (5). In an LCAO analysis these values result in a spin localization of 4% at the antimony atom. As shown in Figure 3, the axial direction of the antimony hyperfine interaction points not towards the dangling bond at all. In a point charge calculation a distant dipole-dipole effect with  $b \approx 200$  kHz results, which is indeed negligible in comparison to the experimentally observed value.

From these examples we may thus conclude that even if the defect geometry is exactly the same, as is the case for the phosphorus- and antimony-vacancy pairs, distant dipole-dipole effects need not to be equally important. In the case of phosphorus it can just be recognized, for antimony it is completely hidden in the much larger hyperfine interaction which results from the LCAO wave function at the impurity atom itself. Yet the "covalent distance" of the dangling bond, four bonds away, along two equivalent paths through two puckered six-rings, is appreciable for both of them.

## V LOCALIZED DEFECTS WITHOUT DANGLING BONDS— TRANSITION METALS

For a number of interstitial transition metal atoms in silicon, ENDOR experiments on  $^{29}\text{Si}$  nuclei have been performed.<sup>7, 31-35</sup> After the first experiment on  $\text{Fe}^0$ , the anisotropic parts of the observed interactions were explained almost completely by distant dipole-dipole interaction with a fully localized spin at the central ion.<sup>31</sup> Afterwards it was found that the correspondence, as illustrated in Table IV, was partly fortuitous, as the signs of the interactions had originally not been determined and turned out not to be the same for all of them.<sup>32</sup> Moreover, at least 25% of spin transfer towards neighboring silicon atoms was found, so that the spin was much more delocalized. Yet, the distant dipole-dipole effect makes an appreciable contribution to many of the observed interactions, as can be inferred from the data in Table IV. This table shows the distances of various (shells of) neighboring atom sites and resulting central dipole-dipole interaction parameters  $b$  under the assumption of 100% spin localization in a point charge at the central impurity ion. For the four different interstitial transition metal systems which have been studied with ENDOR the experimental values for  $b$  are given as well. Most of the interactions are axially symmetric, pointing towards the central ion. Those for which this is not the case are marked in the table.

For an analysis of the observed hyperfine interactions, the LCAO description, as introduced by Watkins and Corbett,<sup>11, 12</sup> was extended in order to comply with the high spin states of the transition metals in silicon.<sup>22, 33</sup> These high spins result from the parallel coupling of the individual spins of the 3d electrons of the transition

TABLE IV

Anisotropic parts  $b$  (in kHz) of the hyperfine interactions of neighboring atoms of interstitial transition metal impurities in silicon, in the approximation of axial symmetry. The calculated distant dipole-dipole interactions under the assumption of 100% spin localization in a central point charge are also given. Spin localizations at the central ions, as calculated in an LCAO approach, are given at the bottom<sup>32-35</sup>

Shell position	d (Å)	100% $b_{dd}$	Fe <sup>0</sup> $b_{exp}$	Fe <sup>+</sup> $b_{exp}$	Ti <sup>+</sup> $b_{exp}$	Cr <sup>+</sup> $b_{exp}$
[1, 1, 1]	2.35	-1250	+1402	(±)1231	(±) 442	-728
[2, 2, 2]	4.70	-156	-196	(±) 226	(±) 678	-332
[2, 2, -2]	4.70	-156	-157		(±) 12	-110
[0, 0, 2]	2.71	-811	-799	(±) 739	(±)3116 <sup>a</sup>	-1352 <sup>a</sup>
[1, 1, -3]	4.50	-178	-434 <sup>b</sup>	(±) 518	(±) 160	-202
[3, 3, 1]	5.91	-78	-85 <sup>b</sup>	(±) 210	(±) 162	-145
[1, 1, 5]	7.05	-46			(±) 44	
[4, 4, 2]	8.14	-30		(±) 130	(±) 66	-84
[4, 4, -2]	8.14	-30			(±) 24	
[2, 2, 6]	9.00	-22			(±) 19	
[5, 5, 1]	9.69	-18			(±) 23	
[5, 5, -3]	10.42	-14			(±) 18	
[0, 2, 4]	6.07	-73		(±) 195	(±) 200 <sup>b</sup>	-133
[1, 3, 5]	8.03	-31		(±) 96	(±) 89 <sup>b</sup>	-47
[0, 4, 6]	9.78	-17			(±) 33 <sup>b</sup>	
[1, 3, 7]	10.42	-14			(±) .24 <sup>b</sup>	
Spin localization at ion:			<75%	<74%	<60%	<78%

<sup>a</sup>Perpendicular axial direction,  $\parallel\langle 110 \rangle$ .

<sup>b</sup>Axial direction  $\parallel\langle 111 \rangle$  instead of central.

ions. For each of these electrons symmetry orbitals were derived, which also included atomic  $s$  orbitals, centrally directed  $\sigma$ -type  $p$ -orbitals, and perpendicular  $\pi$ -type  $p$ -orbitals at the neighboring silicon atoms.<sup>33</sup> In this way a "many"-one-electron LCAO description was obtained. The resulting symmetry orbitals depended on the symmetry of the neighbor sites and on the  $d$ -electron configuration of the transition ion. In some cases just a  $\sigma$  admixture was allowed, in others just  $\pi$  admixture. Mostly, however, symmetry allowed both types of admixture.<sup>7</sup>

For low-symmetry neighbor sites, the axial directions of experimental hyperfine interactions can only be identified as centrally directed, if the interaction can be assigned to a particular lattice site. For Ti<sup>+</sup> this could be achieved for the interactions with lattice sites in a {011} mirror plane of the lattice. If the axial directions which are all in this plane are drawn like in Figure 4, it was found that most of them pointed almost directly towards a particular lattice site. On this phenomenological basis assignments with lattice sites were made for the so-called M-type interactions.<sup>33</sup> Similarly a strong preference for central axial directions was also identified for Cr<sup>+</sup><sup>34</sup> and Fe<sup>+</sup>.<sup>35</sup> In these cases the phenomenon was not just restricted to mirror-plane interactions, but also valid for interactions with atoms at general lattice positions. Therefore we conclude that a particular preference for  $\sigma$  admixture exists. Moreover  $\sigma$  admixture and distant dipole-dipole interaction enhance each other. Table IV shows that in many cases this interaction even makes an important contribution to the value of  $b$ .

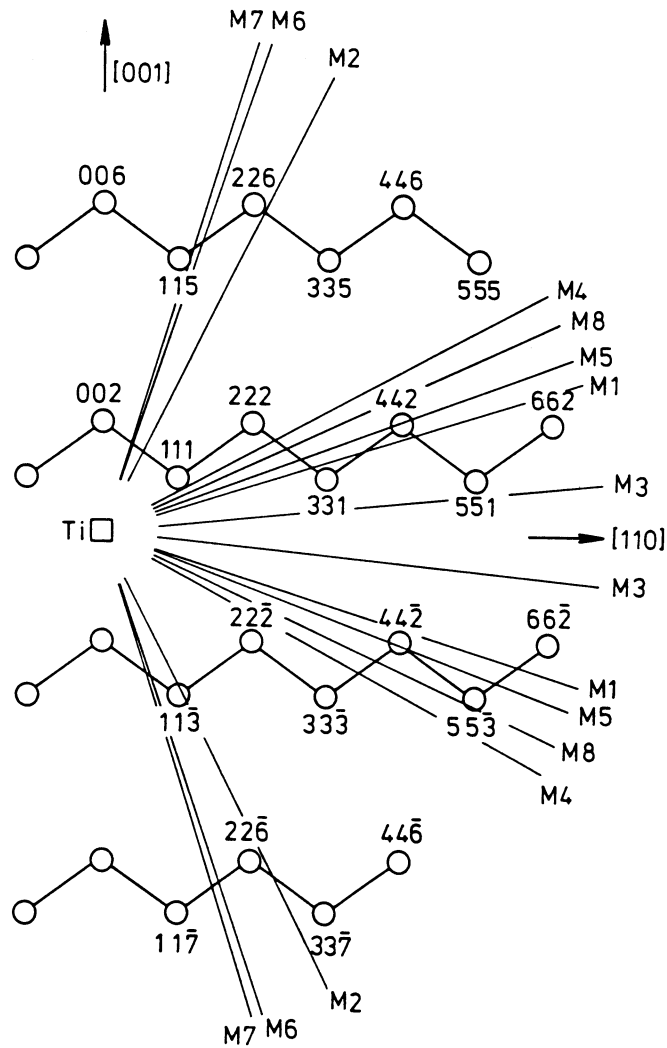


FIGURE 4  $[0\bar{1}1]$  mirror plane of the silicon lattice with an interstitial transition metal ion. Indicated are axial directions of observed hyperfine interactions with  $^{29}\text{Si}$  nuclei around  $\text{Ti}^+$ .

In this way the phenomenon of distant dipole-dipole interaction assisted decisively in the assignment of hyperfine interaction tensors to particular lattice sites. Moreover, indirectly, it played a role in the final determination of the amount of spin localization in LCAO wave functions at the neighbors of the transition ions.<sup>32-35</sup>

## VI SUMMARY

In this paper we assessed the relative importance of distant dipole-dipole effects on the observed hyperfine interactions. This contributed to the insight in the atomic and electronic structure of various imperfections in silicon, which Corbett

considered as one of the main objectives for studies of imperfections in semiconductors.<sup>36</sup>

1) Observed <sup>29</sup>Si hyperfine interactions could be identified with lattice sites in the forbidden plane of the vacancy and the oxygen-vacancy complex and with several neighbor shells of interstitial transition metal impurities.

2) A lattice relaxation opposite to theoretical predictions was derived for the vacancy.

3) Positions of impurity atoms in several impurity-vacancy complexes could be established more reliably through an explanation of the observed impurity hyperfine interactions.

#### REFERENCES

1. J. W. Corbett, J. C. Bourgoin, L. J. Cheng, J. C. Corelli, Y. H. Lee, P. M. Mooney, and C. Weigel, in: *Radiation Effects in Semiconductors*, 1976, N. B. Urli and J. W. Corbett (Eds.) (The Institute of Physics, Bristol, 1977), p. 1 ff.
2. J. W. Corbett, R. L. Kleinhenz, and You Zhi-pu, in: *Defect complexes in Semiconductor Structures*, J. Giber, F. Belezny, I. C. Szép, and J. László (Eds.) (Springer, Berlin, 1983), p. 11 ff.
3. E. G. Sieverts, *Phys. Status Solidi (b)* **120**, 11 (1983).
4. J. W. Corbett, J. C. Corelli, U. Desnica, and L. C. Snyder, in: *Microscopic Identification of Electronic Defects in Semiconductors*, N. M. Johnson, S. G. Bishop, and G. D. Watkins (Eds.) (Materials Research Society, Pittsburg, 1985), p. 243 ff.
5. C. A. J. Ammerlaan, M. Sprenger, R. van Kemp, and D. A. van Wezep, in Ref. 4 p. 227 ff.
6. C. A. J. Ammerlaan, M. Sprenger, and E. G. Sieverts, in: *Defects in Crystals*, E. Mizera (Ed.) (World Scientific, Singapore, 1987), p. 173 ff.
7. E. G. Sieverts, D. A. van Wezep, R. van Kemp, and C. A. J. Ammerlaan, *Materials Science Forum* **10-12**, 729 (1986).
8. G. D. Watkins, J. W. Corbett, and R. M. Walker, *J. Appl. Phys.* **30**, 1198 (1959).
9. G. Feher, *Phys. Rev.* **114**, 1219 (1959).
10. J. G. de Wit, E. G. Sieverts, and C. A. J. Ammerlaan, *Phys. Rev. B* **14**, 3494 (1976).
11. G. D. Watkins and J. W. Corbett, *Discussions Faraday Soc.* **31**, 86 (1961).
12. G. D. Watkins and J. W. Corbett, *Phys. Rev.* **121**, 1001 (1961).
13. J. R. Morton and K. F. Preston, *J. Magn. Resonance* **30**, 577 (1978).
14. E. G. Sieverts, S. H. Muller, and C. A. J. Ammerlaan, *Phys. Rev. B* **18**, 6834 (1978).
15. E. G. Sieverts, *J. Phys. C* **14**, 2217 (1981).
16. M. Sprenger, S. H. Muller, E. G. Sieverts, and C. A. J. Ammerlaan, *Phys. Rev. B* **35**, 1566 (1987).
17. R. van Kemp, E. G. Sieverts, and C. A. J. Ammerlaan, submitted to *Phys. Rev. B*.
18. E. G. Sieverts and C. A. J. Ammerlaan, in Ref. 1, p. 213 ff.
19. M. Sprenger, R. van Kemp, E. G. Sieverts, and C. A. J. Ammerlaan, *Phys. Rev. B* **35**, 1582 (1987).
20. G. D. Watkins and J. W. Corbett, *Phys. Rev.* **134**, A1359 (1964).
21. E. L. Elkin and G. D. Watkins, *Phys. Rev.* **174**, 881 (1968).
22. G. W. Ludwig and H. H. Woodbury, *Solid State Phys.* **13**, 223 (1962).
23. C. A. J. Ammerlaan and J. C. Wolfrat, *Phys. Status Solidi (b)* **89**, 541 (1978).
24. R. van Kemp, M. Sprenger, E. G. Sieverts, and C. A. J. Ammerlaan, submitted to *Phys. Rev. B*.
25. G. A. Baraff, E. O. Kane, and M. Schlüter, *Phys. Rev. B* **21**, 5662 (1980).
26. U. Lindelfelt, *Phys. Rev. B* **28**, 4510 (1983).
27. M. Scheffler, J. P. Vigeron, and G. B. Bachelet, *Phys. Rev. B* **31**, 6541 (1985).
28. Y. H. Lee and J. W. Corbett, *Phys. Rev. B* **8**, 2810 (1973).
29. E. G. Sieverts, Thesis, University of Amsterdam, 1978.
30. G. D. Watkins, *Phys. Rev. B* **13**, 2511 (1976).
31. S. Greulich-Weber, J. R. Niklas, E. R. Weber, and J. M. Spaeth, *Phys. Rev. B* **30**, 6292 (1984).
32. D. A. van Wezep, T. Gregorkiewicz, E. G. Sieverts, and C. A. J. Ammerlaan, *Phys. Rev. B* **34**, 4511 (1986).
33. D. A. van Wezep, R. van Kemp, E. G. Sieverts, and C. A. J. Ammerlaan, *Phys. Rev. B* **32**, 7129 (1985).
34. R. van Kemp, E. G. Sieverts, and C. A. J. Ammerlaan, *Phys. Rev. B* **36**, 3528 (1987).
35. J. J. van Kooten, E. G. Sieverts, and C. A. J. Ammerlaan, *Phys. Rev. B* **37**, 8949 (1988).
36. J. W. Corbett, in: *Defects and Radiation Effects in Semiconductors*, 1978, J. H. Albany (Ed.) (The Institute of Physics, Bristol, 1979) p. 579.